

Self-assembled large-area Co(OH)₂ nanosheets/ionic liquid modified graphene heterostructures toward enhanced energy storageXiao-lei Huang,^{ae} Jia Chai,^{be} Tao Jiang,^c Ying-Jin Wei,^d Gang Chen,^d Wan-qiang Liu,^a Dongxue Han,^{*b} Li Niu,^b Limin Wang^a and Xin-bo Zhang^{*a}

Received 21st October 2011, Accepted 22nd November 2011

DOI: 10.1039/c2jm15377g

Large-area Co(OH)₂ nanosheets have been successfully coated with ionic liquid modified graphene *via* a general strategy. The advantageous combination of graphene and the 2D structure of the Co(OH)₂ nanosheets endows the obtained heterostructures with a remarkable lithium-storage performance, including high reversible capacity and superior cyclic and rate performance.

1. Introduction

Reversible electricity storage using rechargeable batteries has been receiving great attention for potential applications in electric vehicles and renewable energy systems.¹ Among all of the advanced battery systems, lithium-ion batteries (LIBs) have successfully captured the portable electronic market. However, when proposing to conquer the upcoming markets for large scale energy storage, a great improvement in storage capacity is urgently needed.² There is a general consensus that the breakthrough for overcoming such limitations will come from moving away from classical intercalation reactions to conversion reactions.^{2b,3} However, even after decades of intensive efforts, the very rapid decay in capacity resulting from the intrinsically large volume variation during the lithium insertion–extraction process still greatly limits the application of conversion-based materials.^{1a,2b}

Cobalt hydroxide, as one of the most important family of functional inorganic materials, has numerous applications in the field of catalysis,⁴ magnetic materials,⁵ and electrochemical capacitors,^{6a-d} as well as promising conversion-based anode materials for LIBs due to its high capacity.^{6e} Unfortunately, like other conversion-based anode materials, the implementation in LIBs is greatly hampered by its terribly poor cycling performance. One of the most promising strategies to tackle this obstacle is to construct hybrid materials with graphene,

possessing not only high surface area and superior electrical conductivity but also excellent mechanical flexibility and high thermal/chemical stability.⁷ In this regard, many types of hybrid materials consisting of graphene and electroactive metal oxide nanoparticles (NPs) such as SnO₂,⁸ CoO/Co₃O₄,⁹ NiO,¹⁰ TiO₂,¹¹ *etc.*, have been fabricated, wherein graphene is employed to buffer the volume changes of the NPs. Unfortunately, the electroactive NPs are still prone to aggregation upon cycling because of non-intimate contact between graphene layers and the electroactive NPs. This leads to a serious decrease in the capacity of metal oxide/graphene composites.^{8,9} To circumvent this problem, confining individual NPs within a single graphene sheet naturally could be an effective strategy, but is still very challenging when ensuring both high electrical conductivity and a low weight fraction of thin graphene layers on the surface of electroactive NPs.¹² To this end, graphene-encapsulated metal oxides NPs derived by mutual electrostatic interactions were firstly obtained *via* surface grafting and chemical reduction under acidic conditions.¹² However, this method is pretty complex and especially not applicable to metal hydroxides due to their dissolution in acid solution. In addition, the necessary post-reducing process also excludes the usage of some very effective reducing agents such as hydroiodic acid¹³ because of the instability of metal oxides and hydroxides under acidic or alkaline conditions. Therefore, development of a general strategy to effectively coat metal hydroxide with functionalized graphene for enhanced cycling stability is of great importance.

Alternatively, the important task of tuning the electrostatic compatibility between graphene and metal hydroxide for successful assembly might be accomplished on functionalization of acidic- and alkaline- resistant graphene. On the other hand, when electroactive materials are in large area 2D structures and successfully coated with graphene, unlike NPs, the unique 2D structure would greatly alleviate the aggregation of electroactive materials. Although decoration of NPs with graphene has been widely shown, it remains unexplored

^aState Key Laboratory of Rare Earth Resource Utilization, Changchun Institute of Applied Chemistry, Chinese Academy of Sciences, Changchun, 130022, China. E-mail: xbzhang@ciac.jl.cn; Fax: +86-431-85262235; Tel: +86-431-85262235

^bState Key Laboratory of Electroanalytical Chemistry, Changchun Institute of Applied Chemistry, Chinese Academy of Sciences, Changchun, 130022, China. E-mail: dxhan@ciac.jl.cn

^cFAW Group Corporation R&D Center, Changchun, 130011, China

^dCollege of Physics and State Key Laboratory of Superhard Materials, Jilin University, Changchun, 130012, China

^eGraduate University of Chinese Academy of Sciences, Beijing, 100049, China

and highly desirable to synthesize active materials with different morphologies and prepare other architectures of metal oxide and hydroxide/graphene heterostructures to achieve higher lithium storage capacity and better cycling performance.

Herein, we describe a general strategy for the fabrication of graphene coated large-area $\text{Co}(\text{OH})_2$ [GC-Co(OH)₂] heterostructures by assembly between positively charged hydroxide nanosheets and negatively charged functionalized graphene, wherein the amine-terminated ionic liquid plays a key role in modifying graphene to tune its electrostatic charge. The advantageous combination of graphene and the 2D structure of $\text{Co}(\text{OH})_2$ nanosheets greatly alleviates not only the expansion but also the aggregation of electroactive materials, which endows GC-Co(OH)₂ with a high performance stable and reversible capacity that is up to 706 mAh g⁻¹ even after 50 cycles, which is almost twice the gravimetric capacity of the state-of-the-art graphite and thus greatly expands the range of anode choices.

2. Experimental section

Materials

Cobalt nitrate ($\text{Co}(\text{NO}_3)_2 \cdot 6\text{H}_2\text{O}$, Aladdin Reagent, AR), Ammonia solution (NH_4OH , 25%, Aladdin Reagent, AR), Methanol (CH_3OH , Aladdin Reagent, AR), Graphite powder (320 mesh, Shanghai Chemicals, China), 3-bromopropylamine hydrobromide ($\geq 98\%$, Aldrich), 1-methylimidazole ($\geq 98\%$, Linhai Kaile Chemicals, China), Potassium hydroxide (KOH, 82%), Hydrazine monohydrate ($\text{H}_4\text{N}_2 \cdot \text{H}_2\text{O}$, 98%, Tokyo Chemical Industry), Acetylene black (Hong-xin Chemical Works), Polyvinylidene fluoride (PVDF, DuPont Company, 99.9%), N-methyl-2-pyrrolidinone (NMP, Aladdin Reagent, AR), Separator (polypropylene film, Celgard 2400), Electrolyte (1 M LiPF_6 in ethylene carbonate (EC) : dimethyl carbonate (DMC) with the weight ratio of 1 : 1, Zhangjiagang Guotai-Huarong New Chemical Materials Co., Ltd).

Synthesis of nanosheet-shaped $\text{Co}(\text{OH})_2$

In a typical procedure, 1 mL of stronger ammonia water (25%) was added to 40 mL of 0.025 M $\text{Co}(\text{NO}_3)_2$ solution slowly (green blue flocculent precipitate). After stirring for about 15 min, the green blue flocculent precipitate was washed with deionized water by centrifugation 3 times. Then the precipitate was transferred into a 50 mL Teflon-lined autoclave, which was filled with solvents (water/methanol = 1/1, v/v) up to 80% of the total volume. Finally, autoclave was sealed and heated at 180 °C for 12 h. The obtained precipitate was collected by centrifugation and washed with deionized water and ethanol, then dried at 80 °C for 24 h.

Preparation of functionalized graphene sheets

Functionalized graphene sheets (GIL) were synthesized by an epoxide ring-opening reaction between graphene oxide (GO) and the amine-terminated ionic liquid (IL-NH₂).¹⁴ This procedure involves three steps: 1) GO was prepared by oxidizing graphite powder based on a modified Hummers method.¹⁵ 2) the

preparation of IL-NH₂: bromide 3-bromo-propylamine hydrobromide (1.1 g, 5 mmol) and 1-methylimidazole (0.395 mL, 5 mmol) were firstly added to 12.5 mL of ethanol, forming a colorless solution which was refluxed under nitrogen for 24 h. Then, the resulting mixture was purified by re-crystallization from ethanol. Finally, the resulting white powder was dried under vacuum at 60 °C overnight. 3) functionalization of graphene (producing GIL): First, IL-NH₂ (10 mg) was added into 10 mL of GO transparent dispersion in water (0.5 mg mL⁻¹). Then, KOH (10 mg) was added into the above mixture and the mixture was subjected to ultrasonic radiation for 30 min. Finally, the mixture was stirred at 80 °C for 24 h. The final product was centrifuged, washed with ethanol and water, and dispersed in water.

Preparation of GIL-coated anode materials [GC-Co(OH)₂]

0.12 g of $\text{Co}(\text{OH})_2$ was added to 20 mL of deionized water and stirred for about 10 min in a beaker. Then, 75 mL of GIL suspension (0.1 mg mL⁻¹) was added to this beaker and subjected to ultrasonic radiation for 10 min. After the ultrasonic radiation, the above mixture was stirred for about 30 min. Finally, the final products were centrifuged and dried for 24 h at a temperature of 80 °C.

Preparation of unfunctionalized chemically reduced graphene

40 mL of GO (in water, 0.05 wt%) was mixed with 40 mL of water, 0.024 mL of hydrazine solution (50% in water) and 0.284 mL of ammonia solution (25% in water) in a 100 mL glass vial. After being stirred for a few minutes, the GO was reduced to graphene by refluxing the mixture for 24 h at 95 °C.

Characterization methods

Powder X-ray diffraction (XRD) measurements were performed on a Rigaku-Dmax 2500 diffractometer with Cu-K α radiation ($\lambda = 1.5405 \text{ \AA}$). Scanning electron microscopy (SEM) was performed on a field emission Hitachi S-4800 instrument, operating at an accelerating voltage of 10 kV. Samples for SEM were prepared by dispersing the as-prepared product in ethanol by sonicating for about 5 min, and then depositing it onto a silicon wafer, attached to SEM brass stub. Transmission electron microscopy (TEM) was performed using a FEI Tecnai G2 S-Twin instrument with a field emission gun operating at 200 kV. Samples dispersed in ethanol were applied onto the Cu grid and dried in air before TEM imaging. Zeta potential (ζ , effective surface charge) was measured by dynamic light scattering (Malvern Nano-ZS, UK). X-ray photoelectron spectroscopy (XPS) analysis was carried on an ESCALAB MK II X-ray photoelectron spectrometer. TG/DTA analyses were performed at a heating rate of 2.5 °C min⁻¹ in flowing air (NETZSCH STA 449F3, Germany). The Brunauer-Emmett-Teller (BET) surface area and porosity were determined by nitrogen sorption using a micromeritics ASAP 2020 analyzer.

Electrochemical measurements

The electrochemical experiments were performed *via* CR2025 coin-type test cells assembled in a dry argon-filled glove

box with both moisture and oxygen content below 1 ppm. The test cell consisted of a working electrode and a lithium foil which were separated by a Celgard 2400 membrane. The electrolyte solution was prepared by dissolving 1 M LiPF_6 in EC-DMC (1 : 1 w/w). The working electrodes were prepared by casting slurry containing 80% active material, 10% acetylene black and 10% polyvinylidene fluoride (PVDF) onto a copper foil. After vacuum drying at 80 °C for about 24 h, the electrode disks ($d = 12$ mm) were punched and weighed. Each electrode has approximately 1–3 mg of active material. Galvanostatic charge–discharge cycling tests were performed using a LAND CT2001A multi-channel battery testing system in the voltage range between 0.01 and 3 V at room temperature. Impedance and cyclic voltammetry (CV) measurements were performed using a VMP3 Electrochemical Workstation (Bio-logic Inc.).

3. Results and discussions

The overall synthetic procedure of GC-Co(OH)_2 can be illustrated as follows: (1) the graphene sheets are functionalized by 1-(3-aminopropyl)-3-methylimidazolium bromide (GIL) to render positive charge. They spontaneously absorb negatively charged hydroxide ions in deionized water, which is demonstrated by its negative zeta potential (−9.4 mV); (2) large area Co(OH)_2 nanosheets are synthesized by a hydrothermal process and, similarly, their surface is positively charged (zeta potential = +48 mV); (3) the GIL with negative charge and Co(OH)_2 with positive charge can be assembled driven by the mutual electrostatic interactions (Fig. 1) in near neutral solution, which is key to prevent Co(OH)_2 from dissolving.

Fig. 2(a) shows photographs of fresh aqueous solutions of unfunctionalized chemically reduced graphene (RG), GIL, and GC-Co(OH)_2 . It can be clearly seen that both GIL and GC-Co(OH)_2 can be well dispersed in water while RG can't. After one hour resting, as shown in Fig. 2(b), GIL is still well dispersed in water, while, importantly, GC-Co(OH)_2 deposits at the bottom of the bottle, leaving an almost transparent aqueous

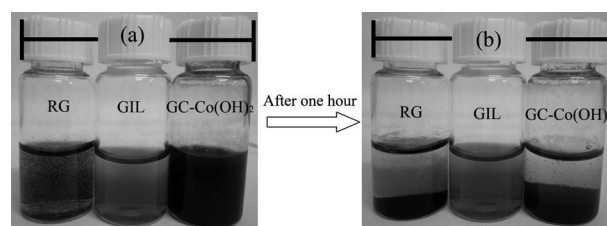


Fig. 2 (a) Photographs of fresh aqueous solutions of unfunctionalized chemically reduced graphene (RG), GIL, and GC-Co(OH)_2 in water, (b) Photographs of RG, GIL, and GC-Co(OH)_2 after one hour.

solution which indicates that almost all the Co(OH)_2 and GIL are fully assembled.

The obtained GC-Co(OH)_2 heterostructures were characterized by X-ray diffraction (XRD) pattern (Fig. 3). Almost all the strong diffraction peaks of the as-prepared GC-Co(OH)_2 can be indexed to a hexagonal structure of Co(OH)_2 (JCPDS card, No. 30-0443). Moreover, it is obvious that the XRD pattern of the GC-Co(OH)_2 exhibits an intense and sharp diffraction peak corresponding to (001) orientation ($2\theta = 19.1^\circ$), indicating a sheet-shaped morphology. Meanwhile, some small amount of Co_3O_4 with cubic structure (JCPDS card, No. 43-1003) can also be found in the sample. Remarkably, no conventional stacking peak for graphene sheets at $2\theta = 26.68^\circ$ is detected.

The morphology and structure of the Co(OH)_2 and GC-Co(OH)_2 were elucidated by scanning electron microscopy (SEM) and transmission electron microscopy (TEM). Fig. 4(a) and 4(b) show that the synthesized Co(OH)_2 is in 2D sheet morphology and irregularly stacked together. The size of each Co(OH)_2 sheet is *ca.* 1–3 μm , and its thickness is less than 30 nm. Note that the smooth surface of the Co(OH)_2 sheets is randomly decorated by a small amount of small NPs which could be assigned to an impurity consisting of Co_3O_4 NPs (Fig. 3). After assembling with GIL, the surface of Co(OH)_2 displays a typical crinkly and rippled structure (Fig. 4(c) and 4(d)), which is quite different from that of as-obtained Co(OH)_2 (Fig. 4(b)). The element distribution in the

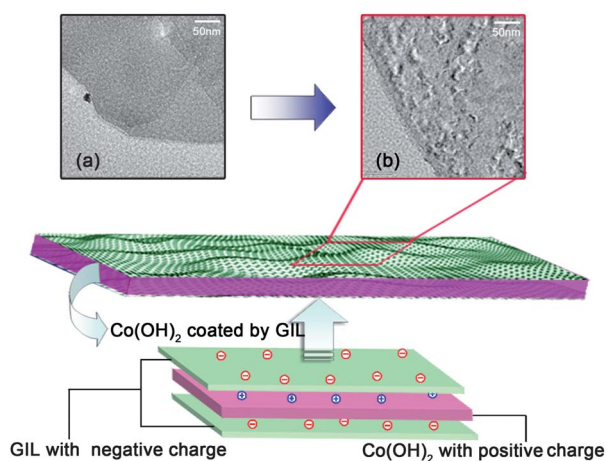


Fig. 1 Schematic diagram of the fabrication of sandwich structured GC-Co(OH)_2 heterostructures driven by the mutual electrostatic interactions between the two species.

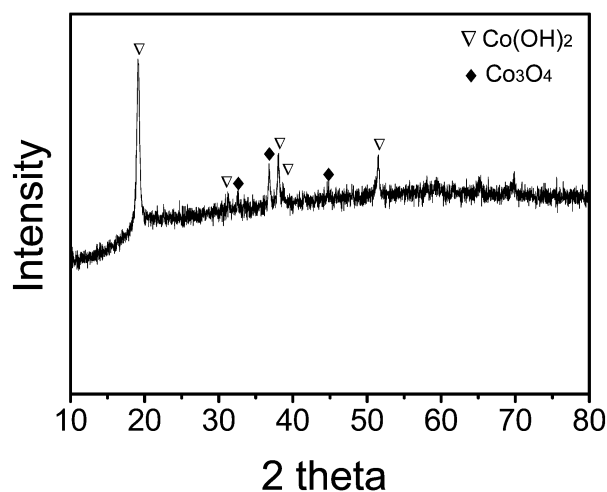


Fig. 3 XRD pattern for GIL-coated Co(OH)_2 nanosheets.

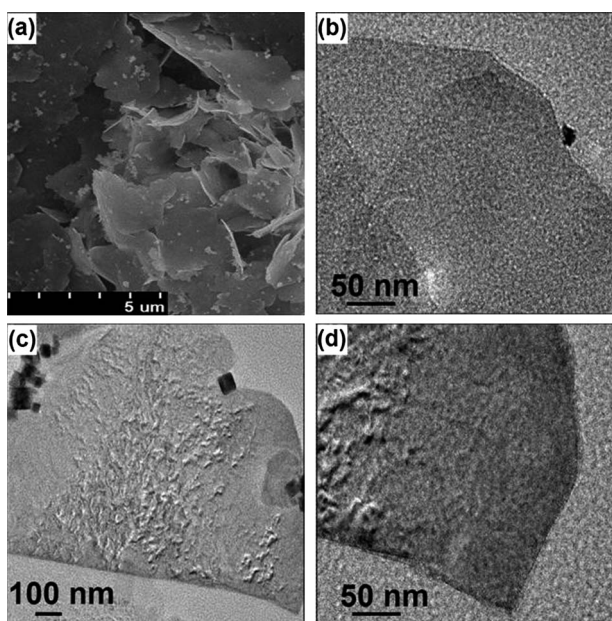


Fig. 4 (a) SEM image of $\text{Co}(\text{OH})_2$, (b) TEM image of $\text{Co}(\text{OH})_2$, (c) TEM image of $\text{GC-Co}(\text{OH})_2$, and (d) magnified TEM image of $\text{GC-Co}(\text{OH})_2$.

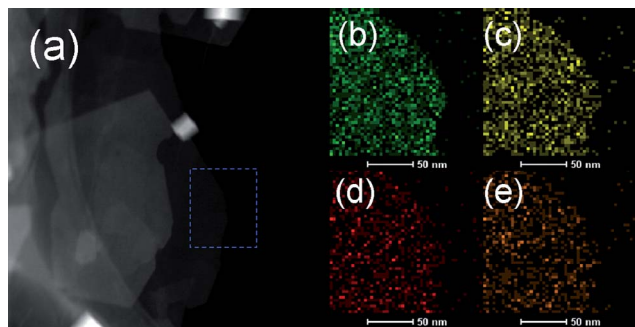


Fig. 5 Elemental mapping images of $\text{GC-Co}(\text{OH})_2$. (a) Typical scanning transmission electron microscopy (STEM) image and corresponding elemental mapping images of (b) cobalt, (c) oxygen, (d) carbon, and (e) nitrogen in the selected area (blue rectangle in (a)).

$\text{GC-Co}(\text{OH})_2$ was analyzed by energy dispersive X-ray (EDX) spectroscopy mapping (Fig. 5). It was found that elements C, Co, O were all present, which is consistent with the intended composite of $\text{GC-Co}(\text{OH})_2$. In addition the element nitrogen is also found on the surface of $\text{GC-Co}(\text{OH})_2$ due to graphene sheets with amine-terminated ionic liquid. The advantageous combination of functionalized graphene and $\text{Co}(\text{OH})_2$ nano-sheets would then effectively buffer the volume change and avoid the aggregation of active materials during the cycle processes (*vide infra*).

To confirm the content of Co_3O_4 NPs, XPS spectrum was measured. However, the high-resolution Co $2p_{3/2}$ spectra of $\text{Co}(\text{OH})_2$ and Co_3O_4 can't be distinguished between 784 and 795 eV due to significant overlaps in binding energy. Therefore, in this study, only the main peaks of $\text{Co}(\text{OH})_2$ and Co_3O_4 are curve-fitted, including the shake-up satellites of the $\text{Co}(\text{OH})_2$ (782.7 eV) in Fig. 6(a).¹⁶ The principle of component analysis

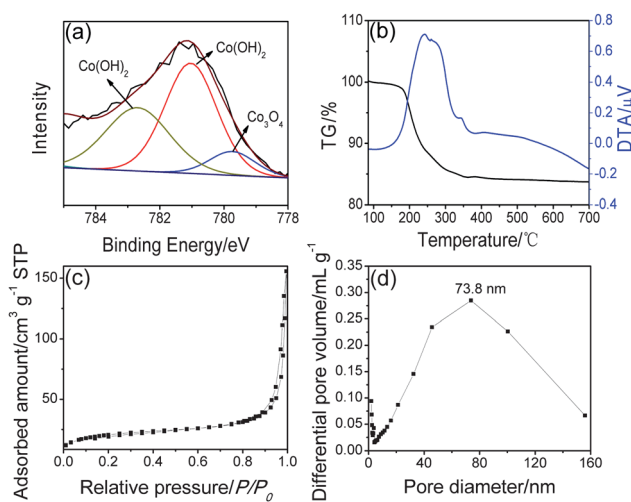


Fig. 6 (a) XPS spectrum of as-obtained $\text{Co}(\text{OH})_2$, (b) TG and DTA curves of the $\text{GC-Co}(\text{OH})_2$, (c) N_2 adsorption-desorption isotherm of the $\text{GC-Co}(\text{OH})_2$, and (d) BJH pore size distribution.

applied to analyze the results quantitatively from the curve-fitted spectra was the ratio of the main peak area of $\text{Co}(\text{OH})_2$ and Co_3O_4 . This can provide quantitative results for the amounts of $\text{Co}(\text{OH})_2$ and Co_3O_4 despite significant overlaps in binding energy. The intense main peaks are at 780.7 eV and 779.9 eV for $\text{Co}(\text{OH})_2$ and Co_3O_4 , respectively.¹⁶ Their area ratio is about 1 : 0.19. Therefore, the content of Co_3O_4 is about 13 wt% in as-obtained $\text{Co}(\text{OH})_2$. Thermogravimetric (TG) analysis and differential thermal analysis (DTA) of the $\text{GC-Co}(\text{OH})_2$ were performed in flowing air (Fig. 6(b)). Clearly, TG analysis indicates approximately 16.5 wt% percentage loss of $\text{GC-Co}(\text{OH})_2$ during calcination in air from 80 to 700 °C. The large exothermic peak between 200 and 350 °C in the DTA profile can be assigned to the formation of Co_3O_4 and the combustion of the graphene. Therefore, the weight change between 80 and 350 °C is due to both the oxidation of $\text{Co}(\text{OH})_2$ and the combustion of graphene. The theoretical value of the weight decrease from $\text{Co}(\text{OH})_2$ to Co_3O_4 is about 14.6 wt%. Thus, the graphene content in $\text{GC-Co}(\text{OH})_2$ hybrid is evaluated to be about 4.4 wt%. The porosity of the $\text{GC-Co}(\text{OH})_2$ heterostructures was evaluated using their N_2 adsorption isotherms (Fig. 6(c) and 6(d)). The Barrett-Joyner-Halenda (BJH) analysis shows that the main pore size is 20 to 160 nm due to decorated Co_3O_4 NPs. The as-prepared $\text{GC-Co}(\text{OH})_2$ heterostructures have a specific surface area (BET) of $70 \text{ m}^2 \text{ g}^{-1}$ and a pore volume of $0.24 \text{ cm}^3 \text{ g}^{-1}$. The advantage of such decorated NPs is that NPs can embed between two layers of large area $\text{Co}(\text{OH})_2$, which then leads to the formation of paths for ion transport between the electrolyte and active material.

The electrochemical activity of $\text{GC-Co}(\text{OH})_2$ was evaluated using cyclic voltammetry (Fig. 7(a)). For comparison, as-obtained $\text{Co}(\text{OH})_2$ was also tested under the same electrochemical conditions (Fig. 7(b)). In the case of $\text{Co}(\text{OH})_2$, two reduction and three oxidation peaks can be clearly observed in the first scanning curve. The first dominant reduction peak is at around 0.85 V, which can be attributed to the reduction reaction of $\text{Co}(\text{OH})_2$ and Co_3O_4 with Li and the formation of solid

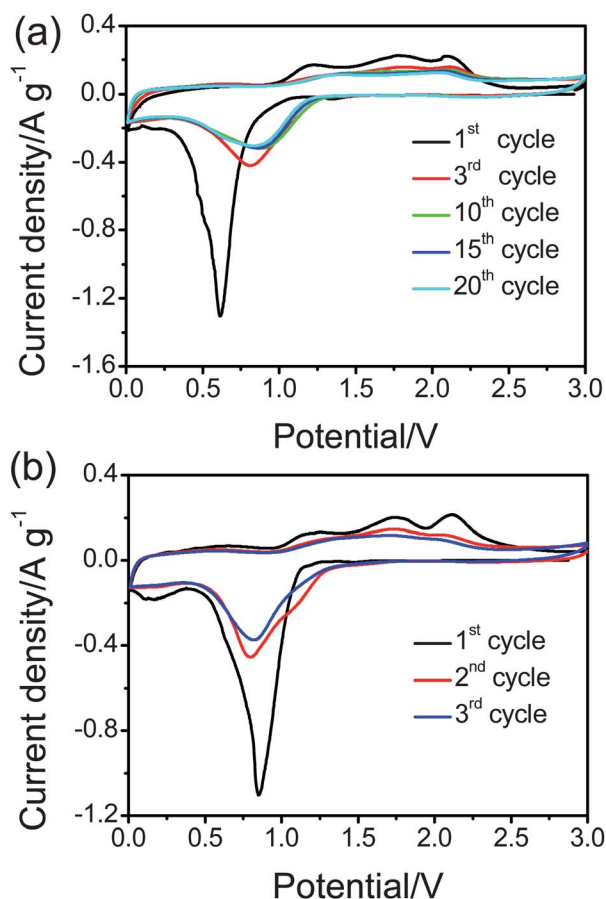


Fig. 7 Cyclic voltammetry of (a) GC-Co(OH)₂ and (b) Co(OH)₂ at a scan rate of 0.1 mV s⁻¹.

electrolyte interphase (SEI) films.¹⁷ A small reduction peak at 0.15 V might be attributed to the formation of lithium dendrites. Three anodic peaks at 1.25, 1.74 and 2.10 V reveal the oxidation of Co from Co⁰ to Co³⁺. These processes are very similar to those of Co₃O₄.¹⁷ It should be noted that the oxidation peaks become much weaker even after only 3 cycles, indicating that the cyclic stability of as-obtained Co(OH)₂ is rather poor. After coating with GIL, it can be found that the first reduction peak shifts to 0.62 V, which might be attributed to functionalized graphene nanosheets on the surface of Co(OH)₂. In the following cycles, the reduction peak shifts to 0.80–0.88 V, which is quite similar to that of the as-obtained Co(OH)₂. Most importantly, it should be noted that both the reduction and oxidation peaks become more and more stable from the third to the 20th cycle, which is in good agreement with its superior cyclic performance (*vide infra*), highlighting again the power of our proposed strategy.

The electrochemical impedance spectra of the GC-Co(OH)₂ and as-obtained Co(OH)₂ are shown in Fig. 8. The typical characteristics of the Nyquist plots are one semicircle in the high frequency range and a sloping straight line in the low frequency range. The radius of the semicircle for the GC-Co(OH)₂ is smaller than that for the as-obtained Co(OH)₂ electrode, indicating that GC-Co(OH)₂ electrode possesses lower contact and charge-transfer impedances. This

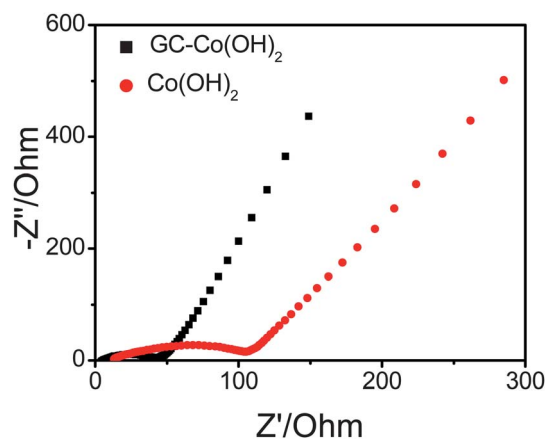


Fig. 8 Nyquist plots of GC-Co(OH)₂ and as-obtained Co(OH)₂ by applying an AC voltage of 5 mV amplitude at 100 mHz to 700 kHz.

result confirmed that the coated functionalized graphene largely improves the electrochemical activity of as-obtained Co(OH)₂.

In a proof-of-concept experiment, coin cells (2025) with a metallic Li counter electrode were used to evaluate the electrochemical performance of the GC-Co(OH)₂ heterostructure. Its capacity and cycle performance were evaluated by galvanostatic charge–discharge measurements between 0.01 and 3 V vs. Li⁺/Li at a current density of 58 mA g⁻¹ (Fig. 9). Typically, it is striking that a large specific capacity of about 1146 mA h g⁻¹ is achieved, and the reversible capacity is 786 mA h g⁻¹ for the first cycle. The reversible capacity of the GC-Co(OH)₂ electrodes is 774 mA h g⁻¹ in the initial 20 cycles and 706 mA h g⁻¹ after 50 cycles. A large irreversible capacity of 360 mA h g⁻¹ is observed for the GC-Co(OH)₂ electrode during the first discharge–charge process (Fig. 9(a)). This can be attributed to the formation of the solid electrolyte interphase (SEI) film at the electrode–electrolyte interface and the reaction of

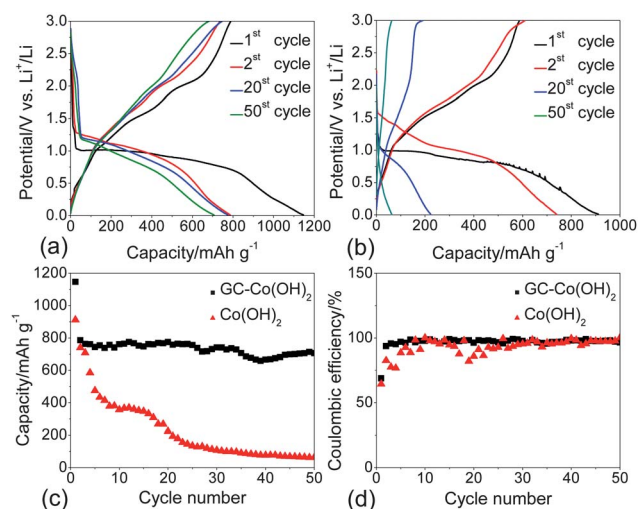


Fig. 9 (a) Charge–discharge curves of GC-Co(OH)₂ and (b) Co(OH)₂, (c) galvanostatic discharge profiles of GC-Co(OH)₂ and Co(OH)₂ at a current density of 58 mA g⁻¹, and (d) coulombic efficiency of GC-Co(OH)₂ and Co(OH)₂.

oxygen-containing functionalized groups on graphene with lithium ions. It should be pointed out that the coulombic efficiencies (Fig. 9(d)) increase to almost unity at successive cycles, indicating that the SEI formed during the first cycle is favourable and stable. For comparison, bare Co(OH)_2 nanosheets were also tested under the same electrochemical conditions (Fig. 9(b)). It exhibits a capacity of 912 mA h g^{-1} in the first discharge process, and the capacity is 223 mA h g^{-1} after 20 cycles (Fig. 9(b)). After 50 cycles, the reversible capacity decreases to only 63 mA h g^{-1} , which is eleven times lower than that of the devices fabricated using the GC- Co(OH)_2 electrode. In addition, the reversible retention capacity (90%) of the GC- Co(OH)_2 electrodes after 50 cycles is much higher than that (9%) of the Co(OH)_2 electrode. The rate performance of GC- Co(OH)_2 and Co(OH)_2 electrodes were evaluated at different charge/discharge rates. As shown in Fig. 10, when compared to bare Co(OH)_2 , the rate performance of GC- Co(OH)_2 is greatly enhanced. Firstly, the LIBs were cycled at 58 mA g^{-1} for 10 cycles, and then the current density was increased in a stepwise manner to 1160 mA g^{-1} for every 10 charge-discharge cycles. Finally, the LIBs were cycled at 58 mA g^{-1} once again. The variation of the specific capacity as a function of cycle number can be clearly observed. The GC- Co(OH)_2 electrode retains a capacity of 220 mA h g^{-1} at a current density of 1160 mA g^{-1} , which is much higher to that of the Co(OH)_2 electrode (30 mA h g^{-1}). Furthermore, when the current density returns to 58 mA g^{-1} , the initial capacity of the GC- Co(OH)_2 can be recovered, while that of the bare Co(OH)_2 electrode can't. The poor electrochemical performance of as-obtained Co(OH)_2 as the anode is caused by its large volume changes, poor electrical conductivity (Fig. 8), and the aggregation of the active material. On the contrary, in the GC- Co(OH)_2 heterostructures, the excellent flexibility of GIL can not only buffer volume changes but also prevents the aggregation of active materials from detaching from the current collector, highlighting again the effectiveness and value of our proposed protocol. These results demonstrate that the prepared GC- Co(OH)_2 has a great potential as a candidate for anode materials for LIBs with high reversible capacity, good cyclic performance and good rate performance.

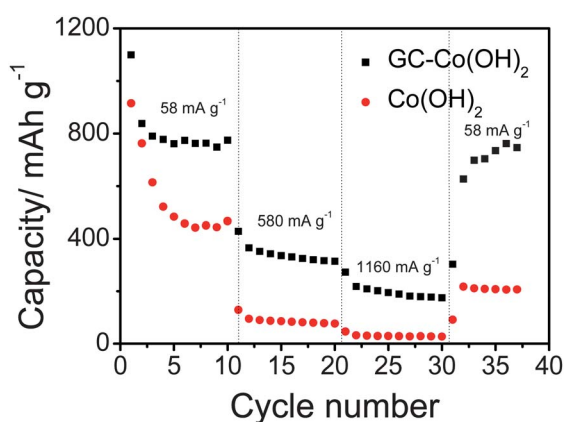


Fig. 10 Rate-capability performance of GC- Co(OH)_2 and Co(OH)_2 .

Conclusions

In summary, we have demonstrated a general strategy to successfully coat large-area Co(OH)_2 nanosheets with ionic liquid modified graphene. The obtained heterostructures could effectively limit and buffer the volume change and provide good conducting pathways during cycling, thus leading to remarkably enhanced lithium-storage performance including highly reversible capacity and superior cyclic and rate performance. The successes in Co(OH)_2 would certainly assist the long-term endeavours to develop high capacity anodes for rechargeable LIBs. We believe that the proposed scalable assembly strategy may be extended to other transition metal oxide and hydroxide materials, which can be used in broad fields including electrochemical capacitors and sensors.

Acknowledgements

This work was financially supported by 100 Talents Programme of The Chinese Academy of Sciences, National Natural Science Foundation of China (Grant No. 21101147), and the Jilin Province Science and Technology Development Program (Grant No. 20100102 and 20116008).

References

- (a) M. Armand and J. M. Tarascon, *Nature*, 2008, **451**, 652; (b) J. B. Goodenough and Y. Kim, *Chem. Mater.*, 2010, **22**, 587; (c) S. Ding, J. S. Chen, D. Luan, F. Y. C. Boey, S. Madhavi and X. W. Lou, *Chem. Commun.*, 2011, **47**, 5780; (d) A. Manthiram, *J. Phys. Chem. Lett.*, 2011, **2**, 176; (e) B. L. Ellis, K. T. Lee and L. F. Nazar, *Chem. Mater.*, 2010, **22**, 691; (f) N. Meethong, Y. H. Kao, W. C. Carter and Y. M. Chiang, *Chem. Mater.*, 2010, **22**, 1088; (g) E. Levi, Y. Gofer and D. Aurbach, *Chem. Mater.*, 2010, **22**, 860; (h) S. W. Lee, N. Yabuuchi, B. M. Gallant, S. Chen, B. S. Kim, P. T. Hammond and S. H. Yang, *Nat. Nanotechnol.*, 2010, **5**, 531; (i) K. Yamamoto, Y. Iriyama, T. Asaka, T. Hirayama, H. Fujita, C. A. J. Fisher, K. Nonaka, Y. Sugita and Z. Ogumi, *Angew. Chem., Int. Ed.*, 2010, **49**, 4414; (j) S. Liu, G. L. Pan, N. F. Yan and X. P. Gao, *Energy Environ. Sci.*, 2010, **3**, 1732.
- (a) C. M. Park, J. H. Kim, H. Kim and H. J. Sohn, *Chem. Soc. Rev.*, 2010, **39**, 3115; (b) J. Cabana, L. Monconduit, D. Larcher and M. R. Palacin, *Adv. Mater.*, 2010, **22**, E170; (c) X. Zhu, Y. Zhu, S. Murali, M. D. Stoller and R. S. Ruoff, *ACS Nano*, 2011, **5**, 3333; (d) V. G. Pol and M. M. Thackeray, *Energy Environ. Sci.*, 2011, **4**, 1904; (e) J. Hassoun, K. S. Lee, Y. K. Sun and B. Scrosati, *J. Am. Chem. Soc.*, 2011, **133**, 3139; (f) Y. Kim, H. Hwang, C. S. Yoon, M. G. Kim and J. Cho, *Adv. Mater.*, 2007, **19**, 92; (g) W. J. Cui, F. Li, H. J. Liu, C. X. Wang and Y. Y. Xia, *J. Mater. Chem.*, 2009, **19**, 7202; (h) H. Uchiyama, E. Hosono, I. Honma, H. Zhou and H. Imai, *Electrochem. Commun.*, 2011, **13**, 8; (i) P. Gao, Y. S. Nuli, Y. S. He, J. Wang, A. I. Minett, J. Yang and J. Chen, *Chem. Commun.*, 2010, **46**, 9149; (j) L. Zhao, Y. S. Hu, H. Li, Z. Wang and L. Chen, *Adv. Mater.*, 2011, **23**, 1385.
- (a) P. Poizat, S. Laruelle, S. Grugeon, L. Dupont and J. M. Tarascon, *Nature*, 2000, **407**, 496; (b) H. Wang, L. F. Cui, Y. Yang, H. S. Casalongue, J. T. Robinson, Y. Liang, Y. Cui and H. Dai, *J. Am. Chem. Soc.*, 2010, **132**, 13978; (c) L. Ji, Z. Tan, T. R. Kuykendall, S. Aloni, S. Xun, E. Lin, V. Battaglia and Y. Zhang, *Phys. Chem. Chem. Phys.*, 2011, **13**, 7170; (d) S. Ding, D. Luan, F. Y. C. Boey, J. S. Chen and X. W. Lou, *Chem. Commun.*, 2011, **47**, 7155.
- M. Dinamani and P. V. Kamath, *J. Appl. Electrochem.*, 2000, **30**, 1157.
- (a) L. Li, H. Qian and J. Ren, *Chem. Commun.*, 2005, 4083; (b) M. Kurmoo, *Chem. Mater.*, 1999, **11**, 3370.
- (a) L. Cao, F. Xu, Y. Y. Liang and H. L. Li, *Adv. Mater.*, 2004, **16**, 1853; (b) C. Yuan, L. Hou, L. Shen, D. Li, F. Zhang, C. Fan, J. Li and X. Zhang, *Electrochim. Acta*, 2010, **56**, 115; (c) J. K. Chang,

- C. M. Wu and I. W. Sun, *J. Mater. Chem.*, 2010, **20**, 3729; (d) W. J. Zhou, J. Zhang, T. Xue, D. D. Zhao and H. L. Li, *J. Mater. Chem.*, 2008, **18**, 905; (e) Y. S. He, D. W. Bai, X. Yang, J. Chen, X. Z. Liao and Z. F. Ma, *Electrochem. Commun.*, 2010, **12**, 570.
- 7 (a) W. S. Hummers and R. E. Offeman, *J. Am. Chem. Soc.*, 1958, **80**, 1339; (b) K. S. Novoselov, A. K. Geim, S. V. Morozov, D. Jiang, M. I. Katsnelson, I. V. Grigorieva, S. V. Dubonos and A. A. Firsov, *Nature*, 2005, **438**, 197; (c) D. A. Dikin, S. Stankovich, E. J. Zimney, R. D. Piner, G. H. B. Dommett, G. Evmenenko, S. T. Nguyen and R. S. Ruoff, *Nature*, 2007, **448**, 457; (d) G. Eda, G. Fanchini and M. Chhowalla, *Nat. Nanotechnol.*, 2008, **3**, 270.
- 8 (a) M. Zhang, D. Lei, Z. Du, X. Yin, L. Chen, Q. Li, Y. Wang and T. Wang, *J. Mater. Chem.*, 2011, **21**, 1673; (b) L. S. Zhang, L. Y. Jiang, H. J. Yan, W. D. Wang, W. Wang, W. G. Song, Y. G. Guo and L. J. Wan, *J. Mater. Chem.*, 2010, **20**, 5462.
- 9 (a) J. Zhu, T. Zhu, X. Zhou, Y. Zhang, X. W. Lou, X. Chen, H. Zhang, H. H. Hng and Q. Yan, *Nanoscale*, 2011, **3**, 1084; (b) B. Li, H. Cao, J. Shao, G. Li, M. Qu and G. Yin, *Inorg. Chem.*, 2011, **50**, 1628.
- 10 H. Liu, G. Wang, J. Liu, S. Qiao and H. Ahn, *J. Mater. Chem.*, 2011, **21**, 3046.
- 11 D. Wang, D. Choi, J. Li, Z. Yang, Z. Nie, R. Kou, D. Hu, C. Wang, L. V. Saraf, J. Zhang, I. A. Aksay and J. Liu, *ACS Nano*, 2009, **3**, 907.
- 12 S. Yang, X. Feng, S. Ivanovici and K. Mullen, *Angew. Chem., Int. Ed.*, 2010, **49**, 1.
- 13 (a) J. Zhao, S. Pei, W. Ren, L. Gao and H. M. Cheng, *ACS Nano*, 2010, **4**, 5245; (b) S. Pei, J. Zhao, J. Du, W. Ren and H. M. Cheng, *Carbon*, 2010, **48**, 4466.
- 14 H. Yang, C. Shan, F. Li, D. han, Q. Zhang and L. Niu, *Chem. Commun.*, 2009, 3880.
- 15 (a) W. R. Collins, E. Schmois and T. M. Swager, *Chem. Commun.*, 2011, **47**, 8790; (b) W. S. Hummers and R. E. Offeman, *J. Am. Chem. Soc.*, 1958, **80**, 1339; (c) N. I. Kovtyukhova, P. J. Ollivier, B. R. Martin, T. E. Mallouk, S. A. Chizhik, E. V. Buzaneva and A. D. Gorchinskiy, *Chem. Mater.*, 1999, **11**, 771.
- 16 J. Yang, H. Liu, W. N. Marterns and R. L. Frost, *J. Phys. Chem. C*, 2010, **114**, 111.
- 17 H. C. Liu and S. K. Yen, *J. Power Sources*, 2007, **166**, 478.